

# A Coupled Ice Sheet–Sea Level Model Incorporating 3D Earth Structure: Variations in Antarctica during the Last Deglacial Retreat<sup>✉</sup>

NATALYA GOMEZ

*Department of Earth and Planetary Sciences, McGill University, Montreal, Quebec, Canada*

KONSTANTIN LATYCHEV<sup>a</sup>

*Physics Department, University of Toronto, Toronto, Canada*

DAVID POLLARD

*Earth and Environmental Systems Institute, The Pennsylvania State University,  
University Park, Pennsylvania*

(Manuscript received 27 May 2017, in final form 1 December 2017)

## ABSTRACT

A gravitationally self-consistent, global sea level model with 3D viscoelastic Earth structure is interactively coupled to a 3D dynamic ice sheet model, and the coupled model is applied to simulate the evolution of ice cover, sea level changes, and solid Earth deformation over the last deglaciation, from 40 ka to the modern. The results show that incorporating lateral variations in Earth's structure across Antarctica yields local differences in the modeled ice history and introduces significant uncertainty in estimates of both relative sea level change and modern crustal motions through the last deglaciation. An analysis indicates that the contribution of glacial isostatic adjustment to modern records of sea level change and solid Earth deformation in regions of Antarctica underlain by low mantle viscosity may be more sensitive to ice loading during the late Holocene than across the last deglaciation.

## 1. Introduction

The potential for marine sectors of the Antarctic Ice Sheet (AIS) to collapse has been recognized for decades (e.g., Mercer 1968, 1978; Weertman 1974; Pollard and DeConto 2009; Alley et al. 2015), and yet the timing and extent of ancient and future retreat remains poorly constrained. One noteworthy example is the recent suggestion that a collapse of the Thwaites Glacier region in West Antarctica, which has the potential to contribute up to about 3 m of global mean sea level (GMSL) equivalent, is already under way (Joughin et al. 2014;

Rignot et al. 2014). Pollard et al. (2015) and DeConto and Pollard (2016) have recently incorporated new mechanisms into their Antarctic Ice Sheet model that accelerate marine ice sheet retreat, and their results suggest that most of the collapse of the Thwaites Glacier could occur over the course of less than a century; on the longer millennial time scale, collapse of the entire West Antarctic Ice Sheet (WAIS) and large sectors of the East Antarctic Ice Sheet (EAIS) is also possible under certain climate warming scenarios.

The stability of the AIS during glacial and interglacial periods is also debated. As an example, the excess volume of the AIS at the Last Glacial Maximum (LGM) relative to present day remains an issue of contention; recent regional modeling of the ice sheet and associated glacial isostatic adjustment (GIA) suggest a GMSL equivalent of less than 8 m during the LGM (Whitehouse et al. 2012; Gomez et al. 2013; Ivins et al. 2013), whereas global GIA models favor values closer to 14–20 m (Lambeck et al. 2014; Peltier et al. 2015). The extent and timing of the collapse of marine sectors of the

<sup>✉</sup> Supplemental information related to this paper is available at the Journals Online website: <https://doi.org/10.1175/JCLI-D-17-0352.s1>.

<sup>a</sup>Current affiliation: Department of Earth and Planetary Sciences, Harvard University, Cambridge, Massachusetts.

*Corresponding author:* Natalya Gomez, [natalya.gomez@mcgill.ca](mailto:natalya.gomez@mcgill.ca)

Antarctic during past warm periods is similarly loosely constrained (Kopp et al. 2013; Hay et al. 2014; Pollard et al. 2015; DeConto and Pollard 2016; Thompson et al. 2011). Clearly, an improved understanding of the response of the AIS to climate changes is necessary to refine these inferences.

A key hurdle in improving our understanding of AIS evolution and its impact on regional and global sea level is to better understand and model the interaction of the ice sheet with the solid Earth. It is well established that ice sheet stability and evolution is strongly influenced by deformation of the solid Earth beneath it and, for marine ice sheets, the depth of water at the grounding line (e.g., Le Meur and Huybrechts 2001; Gomez et al. 2010, 2012). Long-term ice sheet modeling studies have generally included a simplified treatment of Earth deformation in response to the changing ice load (e.g., Le Meur and Huybrechts 2001; Fastook and Prentice 1994; DeConto and Pollard 2016; Golledge et al. 2015). A series of recent studies have now applied more sophisticated coupled ice sheet–sea level–solid Earth deformation models to show that local sea level changes in response to ice mass variations have a stabilizing influence on the past (e.g., Gomez et al. 2010, 2012, 2013; de Boer et al. 2014; Konrad et al. 2014; Pollard et al. 2017) and future (e.g., Gomez et al. 2015; Konrad et al. 2015; Pollard et al. 2017) evolution of the AIS, reducing the rate and extent of ice loss and gain in these regions, and altering predictions of relative sea level (RSL) and crustal deformation.

Coupled modeling yields self-consistent predictions of ice sheet, sea level, and solid Earth variations that may be compared to available geological and geodetic datasets. However, Antarctica is a particularly complex setting, with critical processes taking place along a range of length and time scales. Moreover, the region is characterized by sparse observational constraints on sea level changes and crustal deformation. In addition, the tectonic setting of the continent reflects strong lateral variability in viscoelastic Earth structure beneath the region (see below), yet, to date all coupled models have assumed a radially varying Earth structure.

The WAIS is underlain by a rift system that initially formed in the Cretaceous and experienced renewed extension during the Cenozoic (e.g., Cande et al. 2000; Dalziel and Lawver 2001; Jordan et al. 2010). The EAIS, in contrast, is underlain by a thick craton, dating to the Precambrian (e.g., Harley 2003). Seismic imaging of Earth structure beneath the region shows remarkable lateral variations in crustal thickness and mantle wave speeds between East and West Antarctica (e.g., Danesi and Morelli 2001; Heeszel et al. 2013, 2016; Chaput et al. 2014; Hansen et al. 2014). In particular, East Antarctica is characterized by thick, relatively uniform lithosphere

and relatively fast seismic wave speeds in the upper mantle, whereas much of West Antarctica is underlain by thin lithosphere and upper mantle characterized by anomalously slow seismic wave speeds (Ritzwoller et al. 2001; Shapiro and Ritzwoller 2004; Morelli and Danesi 2004; Heeszel et al. 2013, 2016). In addition to the east–west dichotomy, a large degree of heterogeneity exists within West Antarctica alone (Heeszel et al. 2016; An et al. 2015b). For example, beneath the Thwaites Glacier region, analysis of Polar Earth Observing Network (POLENET) seismic data reveals crustal thickness variations of more than 10 km over a distance of approximately 100 km (Ramirez et al. 2016), and differences in upper mantle shear wave speeds suggest variations in mantle viscosity of about two orders of magnitude (from  $\sim 10^{19}$  to  $\sim 10^{21}$  Pa s).

Models of ongoing GIA across the Antarctic in response to the last ice age that have incorporated 3D variations in mantle structure indicate that the time scale of deformation can vary by several orders of magnitude across the region (Kaufmann et al. 2005; A et al. 2013; van der Wal et al. 2015). Moreover, Hay et al. (2017) investigated the impact of 3D viscoelastic structure on sea level fingerprints of a future collapse of the West Antarctic Ice Sheet and demonstrated that these changes can diverge significantly from simulations adopting a purely elastic Earth model on time scales as short as a few decades. In regard to coupled ice sheet–solid Earth deformation models, complexity in viscoelastic structure will impact predictions of RSL change and crustal deformation both directly, by impacting the time scale and spatial pattern of Earth deformation, and indirectly, by altering, via the sea level feedback, the timing and extent of ice mass variations that load the crust.

The goal of this study is to present, for the first time, a coupled ice sheet–sea level–solid Earth (i.e., GIA) deformation model that incorporates realistic 3D variability in viscoelastic mantle structure beneath the AIS. We apply the model to assess the importance of including this level of complexity in modeling the history of the ice sheet since 40 ka and in estimating the correction for ongoing GIA applied to modern geodetic data. The 3D GIA modeling is computationally challenging, and coupling it to a 3D ice sheet model compounds this challenge. We outline an iterative scheme that addresses this issue and that will be useful for future coupled models of AIS evolution.

## 2. Methods

### *a. Ice sheet and 3D Earth–sea level modeling*

In this study, we present the results of simulations in which we couple an Antarctic ice sheet/shelf model to a

global sea level model that incorporates 3D variations in Earth structure. The two models and the coupling procedure are described below.

The ice sheet model we adopt is described in detail in [Pollard and DeConto \(2012\)](#). We consider this model to be state-of-the-art for long time scale simulations, and it has been employed in a number of recent ice age modeling studies (e.g., [Pollard et al. 2015, 2017](#); [Gomez et al. 2013](#); [DeConto and Pollard 2016](#)). We used the same ice model in the coupled ice sheet–sea level simulations discussed in [Gomez et al. \(2013\)](#), and in the present study, we adopt the same parameters and climate forcing adopted in that earlier work. As in this previous work, basal sliding coefficients in regions characterized by ocean or floating ice in the modern are given a value of  $10^{-5} \text{ m a}^{-1} \text{ Pa}^{-2}$ . Basal sliding parameters in these regions are uncertain, and this value is within a range consistent with available constraints ([Pollard et al. 2016](#)). The ice thickness changes that are passed from the ice model to the sea level model are computed at a spatial resolution of 20 km.

We compute sea level changes using the 3D, finite volume sea level and Earth deformation software described in [Latychev et al. \(2005\)](#), with a recent update that allows for regional grid refinement within a lower-resolution global model. The grid refinement algorithm is described in the supplemental material and has recently been applied in [Goldberg et al. \(2016\)](#) and [Hay et al. \(2017\)](#). This extension is important when considering regions, such as the Antarctic, with strong lateral variability in Earth structure. In the present study, the region of grid refinement extends over the South Pole up to around 60°S and from the surface downward to the base of the upper mantle. The refined grid has an average spatial resolution of 6 km near the surface, decreasing to approximately 50 km below 350-km depth. This spatial resolution is considerably higher than has been adopted in previous models of GIA in Antarctica incorporating 3D Earth structure ([van der Wal et al. 2015](#); [An et al. 2015b](#); [Kaufmann et al. 2005](#)). The gravitationally self-consistent sea level calculations incorporate time-varying shorelines and viscoelastic deformation of the solid Earth in response to changes in surface mass (i.e., ice and ocean) loading. The calculations do not include rotational effects, but tests not shown here with a sea level model adopting one-dimensional (1D) Earth structure demonstrate that local to the Antarctic, rotational effects on sea level and Earth deformation are negligible compared to deformational and gravitational effects in the types of simulations considered here. The 3D viscoelastic Earth structure adopted in the sea level calculations is described in [section 2c](#).

## b. Coupling procedure

In previous work (e.g., [Gomez et al. 2013](#)), we coupled an ice sheet model to a sea level model by invoking the latter to compute changes in the bedrock topography, as required by the ice model, at specified time intervals throughout the simulation. Since the sea level change at a given time in the simulation depends on the full surface loading history up to that time in the simulation, our original coupling method required that the full history of ice and ocean loading changes be read in, and the sea level model be run from the initial to the current time, every time the sea level model was called by the ice sheet model. Furthermore, since the topography at the start of the simulation is unknown a priori, an initial guess for the starting topography is made, and this guess is iteratively improved by performing a full, coupled model simulation extending over the entire time history of the loading, computing the difference between the predicted modern topography and observed modern topography, using this difference to improve the starting topography, and repeating the process until convergence. These earlier sea level calculations (e.g., [Gomez et al. 2013](#)) assumed a 1D (radially varying) viscoelastic Earth structure and adopted a computationally fast, pseudospectral algorithm for solving the so-called sea level equation ([Kendall et al. 2005](#)) that was ultimately based on Love number theory ([Peltier 1974](#)). Since 3D GIA and sea level modeling are far more computationally intensive, we have developed a new computational algorithm that makes coupled modeling feasible. The steps in the computation, which extend over 40 ka, are as follows:

- 1) Global topography at 40 ka and ice thickness changes from 40 ka to modern, as predicted from a previous coupled simulation assuming 1D Earth structure ([Gomez et al. 2013](#)), are passed to the 3D sea level model. The coupled model computed the Antarctic ice history in this previous simulation; the ice history over the rest of the globe was taken from the model ice history ICE5G ([Peltier 2004](#)).
- 2) Using the initial topography and ice thickness changes converged on by either the 1D solution discussed in step 1 for the first iteration or by step 6 in following iterations, the 3D sea level model computes the change in sea level (equivalent to the negative of bedrock/land elevation change relative to the sea surface geoid) globally from 40 ka to the modern. (Note that at this stage, the predicted modern bedrock topography does not match the observed bedrock topography.)
- 3) The sea level changes over Antarctica from step 2 are extracted, interpolated to the ice model grid, and combined with the initial topography in Antarctica

at 40 ka from step 1 to compute a new bedrock elevation history for Antarctica on the ice model grid.

- 4) Next, a correction, given by the difference at each grid point globally between the predicted modern bedrock topography from step 2 and the observed modern bedrock topography [given by BEDMAP2 in Antarctica (Fretwell et al. 2013) and ETOPO2 globally], is applied to each step of the bedrock elevation history computed from step 3. After this correction is applied, the predicted modern bedrock elevation matches the observed. Note that this topographic correction procedure is widely applied in ice age sea level modeling (e.g., Kendall et al. 2005) with a fixed ice history and has also been applied in a coupled dynamic ice sheet–sea level modeling context [e.g., see discussion of Gomez et al. (2013) above].
- 5) The ice model adopts this new, corrected bedrock elevation history in Antarctica and computes new ice thickness changes from 40 ka to the modern.
- 6) The new ice loading history from step 5 and the starting bedrock topography at 40 ka from step 4 are passed to the 3D sea level model.
- 7) Steps 2–6 are repeated, iteratively improving the topography and ice loading history until the ice and bedrock elevation histories converge.

All fields passed between the two models are computed every 200 years. Comparative tests of this new coupling method and the original method described in Gomez et al. (2013) are presented in Fig. S1 of the supplemental material and indicate that the two methods are largely in agreement.

### c. Earth models

The Earth model we adopt assumes an elastically compressible, Maxwell viscoelastic rheology. The elastic and density structure of the model is given by the 1D seismic model Preliminary Reference Earth Model (PREM; Dziewonski and Anderson 1981), and the model incorporates 3D variability in the thickness of an elastic (effectively infinite viscosity) lithosphere and the mantle viscosity.

We adopt the same 3D viscosity model as in Hay et al. (2017). We describe the development of the model in detail in the supplemental material, and we summarize its main features here. The viscosity model is constructed based on results from a range of recent seismic datasets with distinct geographical coverage and resolution. Figure 1a shows the regions in which these different datasets are applied in our model. The lithospheric thickness model of An et al. (2015a) is

adopted for most of the Antarctic plate (regions A2 and A1 of Fig. 1a), and the model of Conrad and Lithgow-Bertelloni (2006), also laterally variable, is adopted for the remainder of the globe (including region A0 in Fig. 1a). These models are scaled to produce a global mean lithospheric thickness of 96 km. The resulting lithospheric thickness variation in the model is shown in Fig. 1b. The mean thickness of the lithosphere is 65 km in West Antarctica and 200 km across the East Antarctic.

The 3D viscosity variation in the model is based on the seismic velocity models of Heeszel et al. (2016) in region A2 and An et al. (2015b) in region A1 and the model named S40RTS (Ritsema et al. 2011) in region A0 and elsewhere (Fig. 1a). The mapping from seismic velocity anomaly to viscosity variability is described in detail in Austermann et al. (2013), and it involves a sequence of mappings from seismic velocity perturbations to temperature anomalies and, finally, a 3D viscosity field. A scaling factor (Austermann et al. 2013) governs the magnitude of the lateral variation in viscosity that also accounts, in the present application, for amplitude differences between the *s*-wave velocities in the three models. We use scaling factors of 0.037, 0.023, and 0.04 for regions A2, A1, and A0, respectively. Figures 1c–g show the resulting viscosity model at a range of depths. Note that the viscosity under the WAIS is characterized by values as low as approximately  $4 \times 10^{18}$  Pa s, reflecting the tectonic setting described in the introduction.

We compare results of simulations based on the 3D Earth model to results derived using an Earth model that assumes a viscosity profile that varies with depth only. This 1D model has a 96-km-thick elastic lithosphere (the average lithospheric thickness across Antarctica in the 3D model) and upper and lower mantle viscosities of  $5 \times 10^{20}$  and  $5 \times 10^{21}$  Pa s, respectively. This model falls within a class of 1D viscosity profiles consistent with GIA-based inferences of mantle viscosity (e.g., Lambeck et al. 1998; Mitrovica and Forte 2004; Lambeck et al. 2014) and is similar to the high viscosity (HV) model in Gomez et al. (2015) and Pollard et al. (2017). Note that both 1D and 3D Earth models were also adopted recently in Hay et al. (2017) to consider the impact of 3D Earth structure on sea level changes following the future collapse of the WAIS.

## 3. Results

### a. Ice cover variations over the last deglaciation

Figures 2a and 2b show Antarctic ice volume changes and the equivalent contribution to global mean sea level



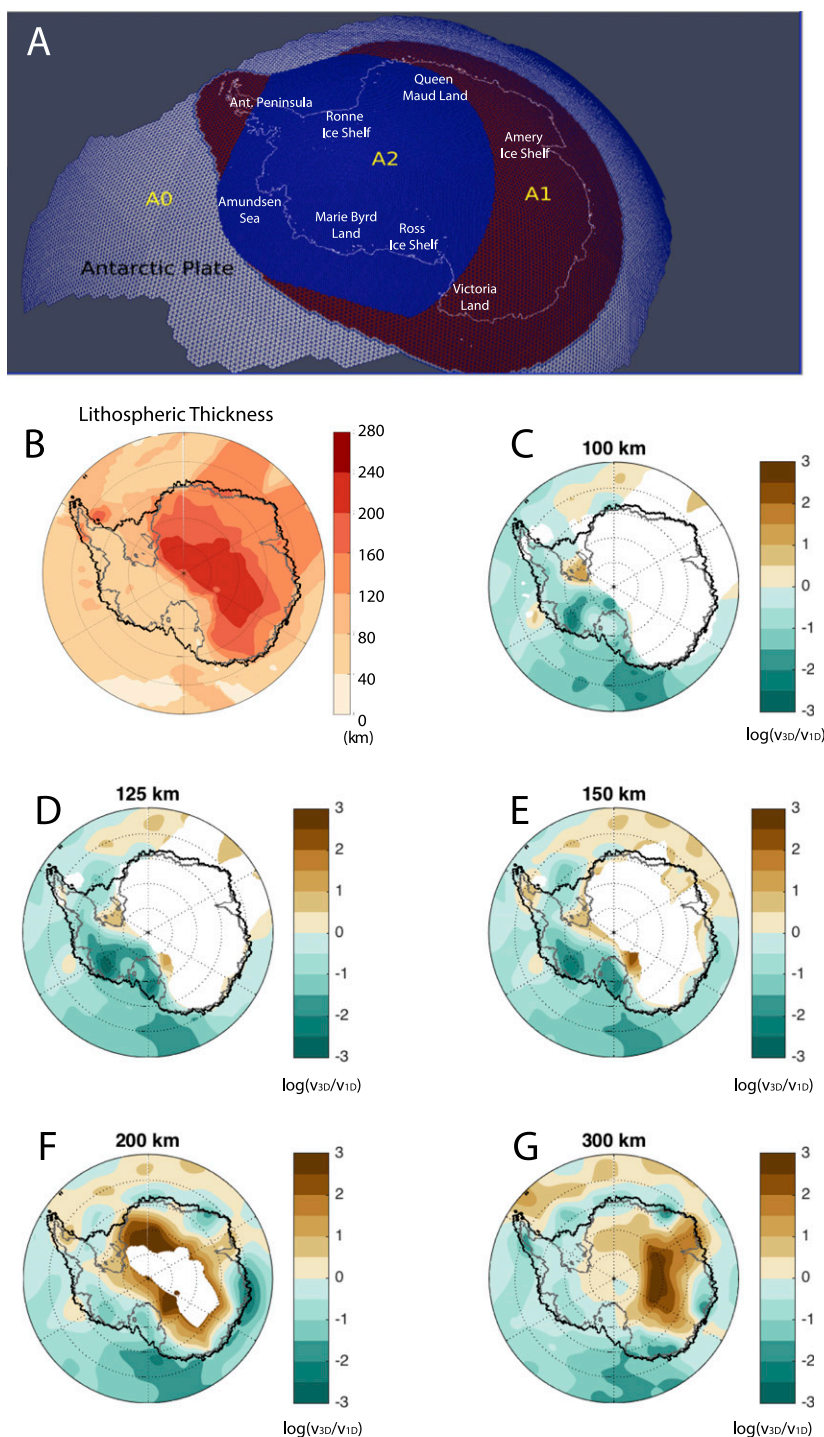


FIG. 1. The 3D viscoelastic Earth model. (a) Regions of the 3D Earth model; S40RTS is adopted globally, including in the light blue region (A0) on the Antarctic plate; the model of [An et al. \(2015b\)](#) is restricted to the dark red area (A1); and the viscosity model of [Heeszel et al. \(2016\)](#) for West Antarctica is restricted to the dark blue area (A2) and is incorporated into the resulting combination of regions A0 and A1. Labels show locations of regions discussed in the text. (b) Lithospheric thickness (km) of the 3D viscoelastic Earth model described in the text. Mantle viscosity variations at depths of (c) 100, (d) 125, (e) 150, (f) 200, and (g) 300 km. Colors represent the logarithm of mantle viscosity in the 3D Earth model relative to the spherically averaged viscosity, 1D Earth model with lithospheric thickness of 96 km, upper mantle viscosity of  $5 \times 10^{20}$  Pa s, and lower mantle viscosity of  $5 \times 10^{21}$  Pa s. Areas in white in (c)–(g) lie within the lithosphere. The black and gray lines in (b)–(g) show the grounding line in the simulation with the 3D Earth model at 20 ka and the modern, respectively.

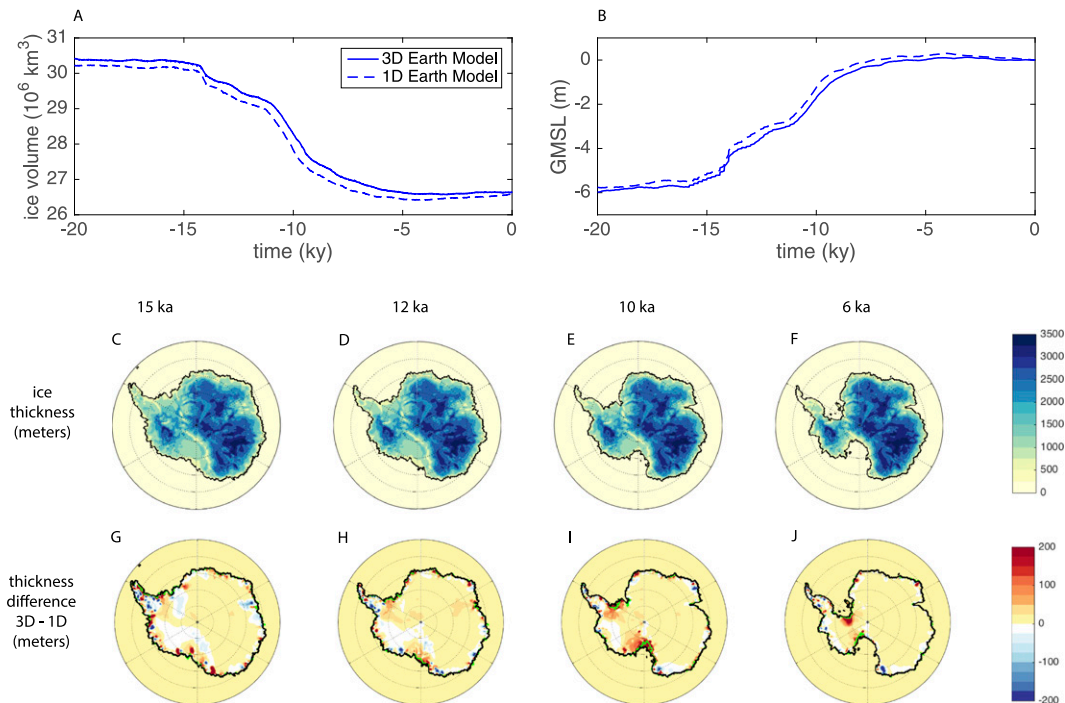


FIG. 2. Antarctic ice cover variations over the last deglaciation. (a) Grounded ice volume changes and (b) GMSL equivalent, relative to the modern, as a function of time, from the AIS over the 20 kyr predicted by the coupled ice sheet–sea level model adopting the 3D (solid blue line) and 1D (dashed blue line) Earth models. Snapshots of Antarctic grounded ice thickness (m) at (c) 15, (d) 12, (e) 10, and (f) 6 ka, predicted from a simulation with the 3D Earth model. (g)–(j) As in (c)–(f), but for differences in grounded ice thickness (m) between simulations using the 3D Earth model and the 1D, radially varying Earth model. Note that the color bar saturates at  $\pm 200$  m to highlight subhundred-meter-scale differences, but localized ice thickness differences of up to approximately  $\pm 1000$  m occur in some regions, in particular where grounding line positions differ. The black lines in (c)–(j) show the grounding line in the simulation with the 3D Earth model at the times indicated. The green lines in (g)–(j) show the grounding line in the simulation with the 1D Earth model. (Note that the grounding lines in the two simulations are overlapping along most of the periphery of the ice sheet, but notable differences occur in the Antarctic Peninsula and the Ross Sea.)

change (calculated by taking the difference in Antarctic ice volume above floatation at a given time in the simulation and at the start of the simulation, converting to a volume of water, and dividing by the area of the modern ocean), respectively, over the last deglaciation predicted from coupled simulations adopting the 1D and 3D Earth models. The impact of incorporating lateral variations in Earth structure on the total ice volume change over the last deglaciation is small. Differences between the two simulations during the deglaciation reach a maximum of  $2 \times 10^3 \text{ km}^3$  of ice or 30 cm of GMSL, where the total change in GMSL over the deglaciation is 6 m. This could be partly because the 3D and 1D Earth structures do not differ significantly in most regions between modern and LGM grounding lines, with the Ross Sea region being an exception (see Figs. 1b–g). The viscosities in the 3D model reach as low as  $5 \times 10^{18} \text{ Pa s}$  and are located under the modern ice sheet in Marie Byrd Land; the grounding line does not pass over this region over the last deglaciation. Additionally, sensitivity studies presented in Pollard et al. (2017), which involve a coupled model and a range of

radially varying Earth viscosity structures, suggest that the contribution from Antarctica to GMSL change over the last deglaciation is less sensitive to the adopted Earth structure than in Pliocene or future simulations.

While the total contribution to GMSL from Antarctica over the deglaciation is not strongly impacted by the incorporation of lateral variations in the Earth model, there are significant regional and local differences in ice cover between the 3D and 1D simulations throughout the deglaciation (Figs. 2c–j). For example, in the Antarctic Peninsula, where the 3D Earth model is characterized by significant lateral variations in viscosity (Figs. 1c–g) and variable lithospheric thickness (Fig. 1b), the difference in ice thickness between the 3D and 1D simulations ranges from  $-200$  to  $1000$  m over relatively small spatial scales on the order of a few hundred kilometers. Along the periphery of the grounded ice in the Ross Sea, the 3D simulation predicts thicker ice by up to about 1 km relative to the 1D simulation and a less-retreated grounding line throughout most of the deglaciation phase (Figs. 2g–i). Viscosities are up to two

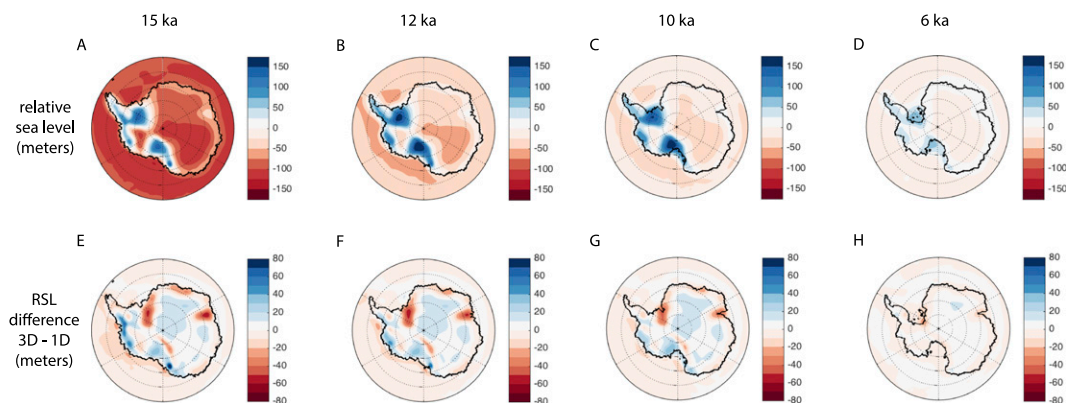


FIG. 3. RSL variations in Antarctica over the last deglaciation. Sea level (m), relative to modern, at (a) 15, (b) 12, (c) 10, and (d) 6 ka, as indicated, predicted from a coupled model simulation adopting the 3D Earth model. (e)–(h) As in (a)–(d), but for differences in relative sea level (m) between simulations using the 3D Earth model and the 1D, radially varying Earth model. The black line in each frame shows the contemporaneous grounding line.

orders of magnitude lower in the 3D Earth model, compared to the 1D model, beneath the Ross Sea region (Figs. 1c–g). Therefore, the solid surface rebounds faster in response to ice unloading in the 3D case, leading to dampened ice loss and slower grounding line retreat in this region (see saturated red regions and difference in grounding line position between the two simulations in Figs. 2g–i). Note that there are significant differences in ice thickness between the 1D and 3D simulations around the entire periphery of the ice sheet. These local differences in ice dynamics between the two simulations feed back onto local surface loading history, which in turn significantly impacts relative sea level and uplift rate predictions. We turn to this issue next.

#### b. Relative sea level changes over the last deglaciation

Figures 3a–d plot maps of RSL change predicted by the coupled model with 3D Earth structure at snapshots in time during the deglaciation. Gomez et al. (2013) review the physics of postglacial sea level changes in detail (see section 3.1 of their supplementary material), and we summarize the key processes contributing to the RSL changes predicted in Fig. 3 here. As climate warms and the ice sheet retreats, the solid Earth rebounds in areas freed of grounded ice; hence, RSL is positive at the LGM in these regions, reaching up to 150 m in the Ronne and Ross Sea regions (blue and white regions in Fig. 3a), and generally falls during the deglaciation (Figs. 3b–d). Crustal subsidence occurs around the periphery of the regions experiencing ice loss, contributing a sea level rise there over the deglaciation (see deepest red regions in Figs. 3a–c). In addition to the local ice cover changes in Antarctica, far-field ice cover changes are also contributing to the pattern of LGM RSL. In particular, the major deglaciation that occurred in the

Northern Hemisphere between 15 and 10 ka contributed a sea level rise across all of Antarctica. This is evident in the overall increase in RSL between Figs. 3a and 3b, including regions that experience ice loss (i.e., peak RSL is higher in Fig. 3b than in Fig. 3a).

Figures 3e–h map differences in RSL between the 3D and 1D simulations at snapshots in time through the deglaciation. RSL predictions differ by up to 80 m at the start of the deglaciation at 15 ka (Fig. 3e), up to 50 m during the deglaciation (Figs. 3f,g), and up to 20 m at the end of the deglaciation at 6 ka (Fig. 3h). The adopted Earth viscosity structure and lithospheric thickness in these simulations impacts the timing and spatial pattern of Earth deformation. Regions of low viscosity in West Antarctica in the 3D simulation rebound faster and reach isostatic equilibrium sooner than the regions with higher mantle viscosity (which lie mainly in the east; see Figs. 1c–g). Furthermore, lowering the viscosity and thinning the elastic lithosphere localizes deformation to the areas experiencing surface loading changes. In areas of ice sheet retreat around the periphery of Antarctica, deformation is more localized to the region near and toward the interior of the grounding line, where much of the ice loss takes place. Note, however, that the pattern of differences in Figs. 3e–h is complex, and the contribution from the differing responses of the two Earth models to surface loading cannot be separated from the contribution from local differences in ice history between the two simulations (see Fig. 2). In addition, differences in the sea level response yield differing bedrock topographies beneath the ice sheet at the start of the simulations at 40 ka in order that the modern topography at the end of the simulation matches the observed topography (see section 2). Note that the sensitivity of the spatial pattern and timing of bedrock deformation to

viscoelastic Earth structure is further explored in coupled simulations adopting a range of 1D radially varying Earth models in both [Gomez et al. \(2015\)](#) and [Pollard et al. \(2017\)](#).

These complex differences in the evolution of topography (or equivalently, sea level) back in time may significantly impact the interpretation of RSL records in Antarctica. Figure S2 in the supplemental material plots RSL predictions from the 3D and 1D simulations at several specific sites with existing RSL records ([Briggs et al. 2013](#); [Hjort et al. 1997](#); [Roberts et al. 2011](#)). Differences between the 3D simulation predictions and records at a given site could be resolved by changing either the local ice sheet model parameters (e.g., increasing the slipperiness of the bed beneath the ice sheet in the region would thin the ice sheet locally) or the regional Earth structure in the simulation, or both. In the following section, we begin to examine the regional sensitivity of the Earth deformation history to these two factors.

### c. Modern crustal motions

Constraining ongoing Earth deformation associated with past ice loss is important for accurately interpreting geodetic data [e.g., Global Navigation Satellite System (GNSS)-measured crustal motions and GRACE gravity data]. We analyze differences in modern bedrock uplift rate predictions between simulations with 1D and 3D Earth structure in [Figs. 4](#) and [5](#). Black dots in [Fig. 4](#) indicate the locations of existing POLENET GPS stations (a subset of the total existing GNSS stations in Antarctica), and we plot uplift rate predictions at these specific sites in [Fig. S3](#) of the supplemental material.

[Figure 4a](#) shows modern bedrock uplift rates across Antarctica predicted from the coupled model simulation based on the 3D Earth model. Modern uplift rates represent a snapshot in time of how the radial position of the solid surface in the simulation is changing at the end of the simulation (i.e., at 0 ka) because of the full history of ice and water loading since the start of the simulation. Regions that experienced substantial ice loss during the simulation are predicted to be uplifting at the modern, reaching up to  $8 \text{ mm yr}^{-1}$  inland of the Ronne Ice Shelf. Minor subsidence occurs in the 3D simulation in the surrounding regions and in the interior of East Antarctica as a result of a combination of ice accumulation through increased snowfall in the interior and peripheral bulge subsidence.

[Figure 4b](#) shows the difference in modern uplift rates predicted from the 3D and 1D coupled model simulations. Incorporating 3D viscosity variations leads to lower uplift rates in much of West Antarctica and along

the periphery of the northern sector of East Antarctica; higher uplift rates in the Antarctic Peninsula and in a localized region of southern Victoria Land (where the uplift rate is close to zero in the 1D case); and less subsidence in the interior of East Antarctica. These differences are associated with differences in the Earth model response, ice sheet evolution, and initial topography between the two simulations. To separate these contributions, we performed an additional simulation with the 3D Earth model, but driven by the ice history and initial topography from the coupled model simulation with the 1D Earth model. [Figure 4c](#) plots the difference in predicted uplift rates between the latter simulation and the coupled simulation with 1D Earth structure. [Figure 4c](#) provides an estimate of the impact of the Earth model on uplift rates. [Figure 4d](#) shows the difference between [Figs. 4b](#) and [4c](#), which effectively shows the influence of ice history and initial topography differences between the 1D and 3D simulations.

The reduced amplitude of predicted uplift rates in regions of marine ice loss in West Antarctica in [Fig. 4b](#) are clearly associated with the different Earth models (blue regions in [Fig. 4c](#), reaching down to  $-3 \text{ mm yr}^{-1}$ ). Viscosities in the 3D Earth model are lower, and the lithosphere is thinner than the average 1D model in these regions ([Figs. 1b–g](#)), so uplift toward isostatic equilibrium following the deglaciation takes place faster. Thus, the system is closer to reaching isostatic equilibrium in the modern. The impact of the Earth model is also responsible for lowering uplift rates in a region along the periphery of East Antarctica between Queen Maud Land and the Amery Ice Shelf. Here, the lithosphere is significantly thicker in the 3D model than in the 1D model ([Fig. 1b](#)), but there is a zone of lower-than-average viscosity extending down from the base of the lithosphere in the 3D model ([Figs. 1f,g](#)). Hence, this region also becomes closer to isostatic equilibrium over a shorter period following deglaciation. In addition, the thicker lithosphere acts to dampen the deformation in general in the East Antarctic.

On the other hand, the higher uplift rates in the 3D simulation in the Antarctic Peninsula and in localized regions of East Antarctica and Victoria Land (red regions in [Fig. 4b](#)) are largely related to differences in ice history and initial topography (see localized red regions in [Fig. 4d](#)). Note that the differences in predicted uplift rates in these localized regions can be significant, reaching over  $10 \text{ mm yr}^{-1}$ . This sensitivity introduces significant uncertainty in the interpretation of GNSS measurements. The 3D structure of the Earth model also influences predicted uplift rates, increasing them by up to  $2 \text{ mm yr}^{-1}$  across much of the Antarctic Peninsula



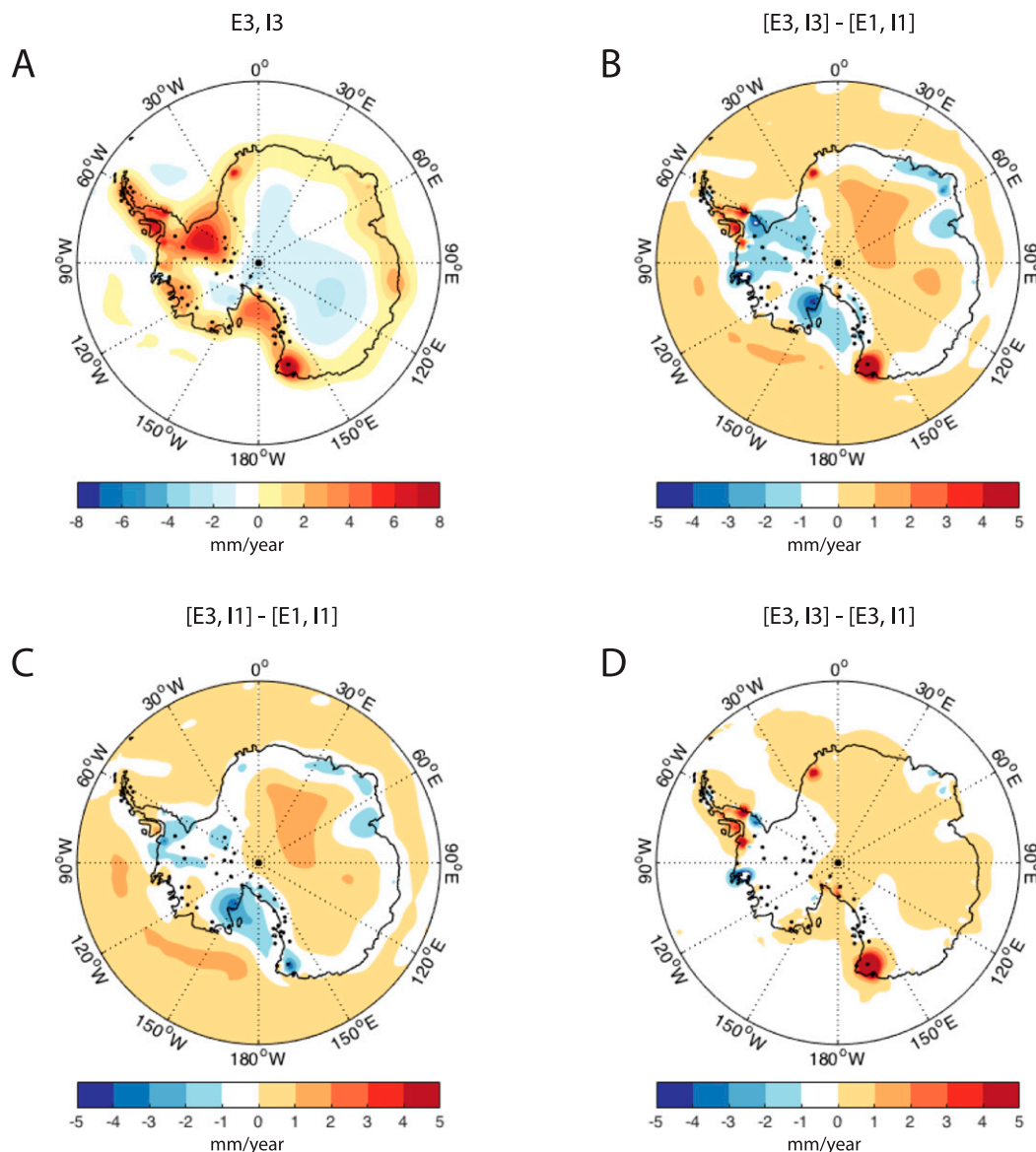


FIG. 4. An analysis of the contributions to predictions of vertical solid Earth uplift rate ( $\text{mm yr}^{-1}$ ). E1 and E3 refer to simulations adopting the 1D and 3D Earth models, respectively, and I1 and I3 refer to ice loading histories predicted from the 1D and 3D coupled simulations, respectively. (a) Modern bedrock uplift rates predicted from the coupled model simulation with the 3D Earth model. Colors represent the rate of change in radial position of the solid surface at 0 ka in the simulation. (b) Difference in modern bedrock uplift rates between simulations adopting the 3D Earth model [plotted in (a)] and the 1D Earth model. (c) An estimate of the contribution to the difference plot in (b) associated with differing Earth model responses. The estimate is calculated by subtracting the uplift rate from a coupled model simulation with the 1D Earth model, from the uplift rate predicted from a sea level simulation with the 3D Earth model driven by the same ice history and initial topography as in the coupled simulation with the 1D Earth model. (d) Difference between (b) and (c), showing an estimate of the contribution to differences in uplift rate between the 3D and 1D coupled model simulations associated with differences in initial topography and ice load history between the two simulations. Black dots on the maps represent the locations of existing POLENET GPS stations (see <http://polenet.org/a-net>).

(Fig. 4c). This region is underlain by variable Earth structure with some areas of higher viscosity (Figs. 1c–g) and, hence, slower response times and more uplift remaining at present.

The difficulty in separating contributions from ice loading changes over the last deglaciation from more recent Holocene ice cover changes presents an important challenge in interpreting modern uplift rate

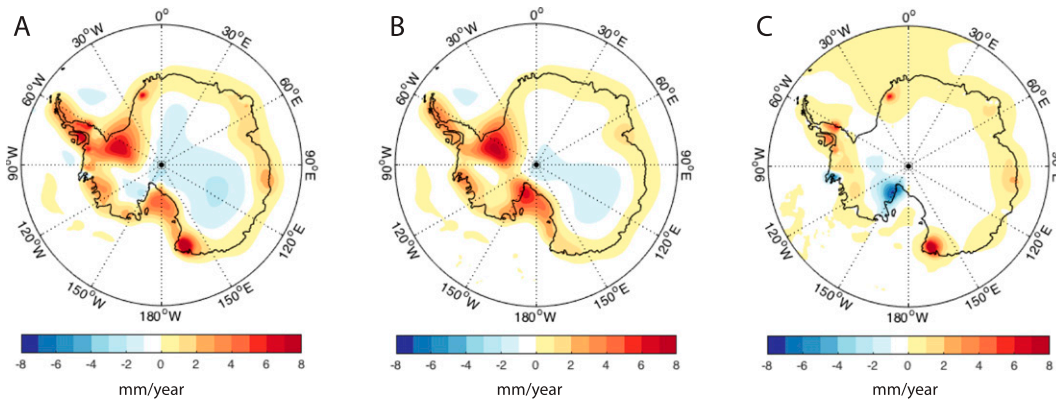


FIG. 5. Contributions to modern bedrock uplift rates ( $\text{mm yr}^{-1}$ ) from deglacial and recent ice cover changes. (a) Identical to Fig. 4a, showing modern bedrock uplift rates predicted from the coupled model with the 3D Earth model. (b) Uplift rate predicted from a sea level simulation adopting the 3D Earth model with initial topography and ice history from the 3D coupled simulation, except that changes in ice history have been zeroed out over the last 3 kyr. This field represents the contribution to the predicted uplift rate in (a) associated with ice cover changes taking place before 3 ka in the coupled model simulation with the 3D Earth model. (c) Difference between the uplift rate predicted with the full coupled model simulation with 3D Earth structure plotted in (a) and (b), representing the contribution to the predicted uplift rate in (a) from ice cover changes over the last 3 kyr.

predictions. In Fig. 5b, we plot uplift rates predicted from a simulation using the sea level model with 3D Earth structure in which we applied the ice history derived from the coupled simulation, but zeroed out changes in ice cover over the last 3 kyr of the simulation. That is, Fig. 5b shows the contribution to modern uplift rates from ice loading changes taking place before 3 ka in the simulation. Figure 5c shows the difference between Figs. 5a and 5b, and it thus reflects the contribution of ice loading changes over the last 3 kyr to the predicted modern uplift rates in the 3D simulation. These results indicated that the large-scale, ice sheet-wide pattern of the modern uplift rate map predicted in Fig. 5a is associated with deglacial ice loading changes (Fig. 5b), but there is also a significant contribution in some regions from more recent changes in ice cover (Fig. 5c). For example, a recent thickening of ice in the Ross Ice Shelf region contributes to subsidence in this region, and recent ice loss in the Antarctic Peninsula and Victoria Land contributes uplift (Fig. 5c). We note that there is a lack of observational constraints on Holocene variations in ice thickness and extent in Antarctica, and our results suggest that improving constraints during this time period may be critical for establishing accurate uplift rate predictions.

Finally, in Fig. 6, we consider the impact of including 3D Earth structure on predictions of horizontal crustal motions. Predicted horizontal crustal velocities in the simulation that includes 3D Earth structure (Fig. 6a) differ significantly in magnitude and direction from those predicted in the simulation adopting the 1D Earth model (Fig. 6b). The motions are generally larger in magnitude in the 3D case, with the greatest deviations in

magnitude and direction (Fig. 6c) occurring in the vicinity of where there are ice loading differences between the two simulations, and vertical crustal uplift rates also differ (cf. peaks in Figs. 6c and 4b). Furthermore, a background east to west trend in the horizontal motions across the whole continent is predicted when 3D Earth structure is included (left-pointing arrows in Fig. 6a) that is not present in the simulation with average 1D Earth structure (Fig. 6b); a similar trend was also found in Kaufmann et al. (2005). As in the case of the radial uplift rates considered in Fig. 4, the impact of including lateral variations in Earth structure on horizontal motions (Fig. 6c) is quite complex, associated with a combination of differences in the predicted ice loading history and the adopted continent-scale and regional-scale lithospheric thickness and viscosity structure. We conclude that careful consideration of 3D Earth structure is needed for the interpretation of measurements of both radial and horizontal crustal motions. Note that 3D structure will also have implications for the interpretation of other geodetic measurements, such as GRACE gravity data; we leave exploring this to future work.

#### 4. Discussion and conclusions

We coupled, for the first time, a gravitationally self-consistent, global sea level model that includes 3D viscoelastic Earth structure to a dynamic ice sheet model and applied the model to simulate ice and sea level changes and solid Earth deformation over the last deglaciation, from 40 ka to the modern. Our results show that the total contribution from Antarctica to sea level change over the last deglaciation is not significantly

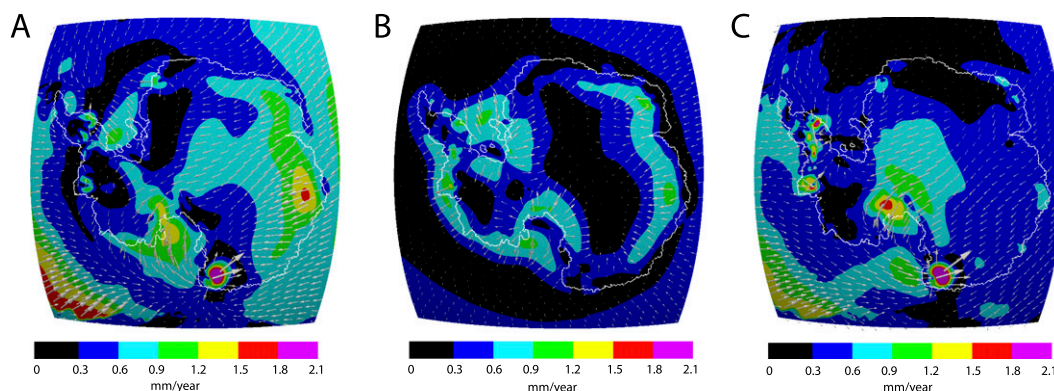


FIG. 6. Predictions of horizontal crustal velocities from coupled model simulations adopting (a) 3D and (b) 1D Earth models. (c) Difference between (a) and (b). White arrows indicate the direction of horizontal motions, and color shading denotes the magnitude ( $\text{mm yr}^{-1}$ ). The white outline in each frame shows the grounding line position at the modern predicted from the coupled model simulation with the 3D Earth model.

altered by the inclusion of 3D Earth structure (Figs. 2a, b). However, significant local differences in ice loading history occurred in our 3D Earth model simulation (Figs. 2g–j) relative to the 1D case, and these differences altered predicted RSL (Figs. 3 and S2) and crustal velocities (Figs. 4–6 and S3), compared to simulations with 1D Earth structure.

A central implication of these results is that better resolution of the viscoelastic structure of the Earth and its response to surface loading is needed in order to advance our understanding of the response of the AIS to climate changes and the contribution of past ice sheet evolution to modern measurements of the ice–Earth system. Seismic models capturing elastic structure under Antarctica are continually being improved as more data become available (e.g., Heeszel et al. 2016), but obtaining high-resolution constraints on Earth structure across the entire Antarctic continent may not be feasible. Our 3D coupled modeling can be used in this case to elucidate regions where ice sheet dynamics are most sensitive to Earth structure and, thus, where higher-resolution data are particularly needed. For example, our results show significant differences in local ice history between the 1D and 3D simulations in the Amundsen Sea Embayment—a region that is also considered particularly susceptible to future climate warming; collecting additional constraints on Earth structure there is thus particularly important.

We also demonstrated that predicted modern uplift rates may be quite sensitive to Holocene ice cover variations, in particular under West Antarctica and regions of East Antarctica, that are underlain by a low viscosity mantle (Fig. 5). In particular, in some localized areas, small adjustments in ice loading over the last few thousand years dominate the signal as a result of GIA. This introduces significant uncertainty into the modern GIA

signal, since the ice model is relatively unconstrained over the late Holocene. That is, the pattern in Fig. 5c would be quite different with a relatively insignificant change in ice model parameters. There are relatively few records of late Holocene ice sheet and sea level changes in Antarctica, in comparison to records over the last deglaciation (e.g., Briggs et al. 2013; Whitehouse et al. 2012). Recent work suggests that there may have been complex ice cover changes in certain areas of the West Antarctic over the Holocene, with retreat beyond modern grounding lines followed by readvance (e.g., Siegert et al. 2013; Bradley et al. 2015). Our results suggest that additional constraints on late Holocene ice cover changes are needed to improve estimates of the contribution of past ice cover changes to modern measurements of ice, sea level, and solid Earth changes around Antarctica.

Figures 2a,b indicate a relatively low sensitivity of the global mean sea level change from the AIS since the LGM to the inclusion of 3D Earth structure. However, sensitivity studies have shown that the contribution of the AIS to global mean sea level change under future and Pliocene climate warming may be significantly more sensitive to the adopted Earth structure (Gomez et al. 2015; Pollard et al. 2017). Indeed, the most extreme low viscosities of  $10^{18}$  Pa s in our 3D Earth model are in regions under the modern Thwaites and Pine Island Glacier regions of the WAIS, rather than in the regions over which the grounding line migrated during the last deglaciation (see Figs. 1c–e). An important next application of this newly developed coupled ice sheet–sea level model with 3D Earth structure will be to investigate the response of the Antarctic Ice Sheet to future warming scenarios.

Finally, it is important to note that in addition to the challenges involved in obtaining high-resolution seismic tomography discussed above, there remains substantial uncertainty in estimating viscosity structure from

seismic tomography. There are several approaches to deriving a model of Earth rheology from seismic results (e.g., Wu and van der Wal 2003; Latychev et al. 2005; van der Wal et al. 2015). The approach taken in this study—outlined in, for example, Latychev et al. (2005)—involves using mineral physics and modeling constraints to map seismic velocity variations to relative perturbations in density, converting to a temperature field through a coefficient of thermal expansion, and finally, assuming an exponential dependence of viscosity on temperature with a scaling factor that dictates the strength of the viscosity–temperature dependence. Each step in the conversion involves an added degree of uncertainty, and quantifying this uncertainty has been identified as crucial to future advances in GIA research (IAG/SCAR-SERCE 2017). The 3D coupled model developed in this study can be used to quantify how uncertainties in rheology translate into uncertainties in predictions of ice and sea level variations and solid Earth deformation.

Our work emphasizes that interactions among ice, sea level, and the solid Earth in Antarctica are complex, dynamic, and challenging to model and constrain. This study begins to quantify the substantial uncertainty in estimates of ice sheet evolution and sea level change introduced by the complex, laterally variable nature of Earth structure beneath Antarctica. The incorporation of lateral variations in Earth structure in a global sea level model requires a substantial increase in computational cost, and large ensemble simulations and parameter explorations with such a model are currently not computationally feasible. Future work will involve applying our state-of-the-art 3D coupled model to identify best-fitting radially varying Earth structure models to adopt in studies of a given region and/or time period and to quantify the uncertainty involved in neglecting lateral variations in these settings. Furthermore, the results presented herein can be used to identify the regions and time periods in which the incorporation of 3D Earth structure is critical for accurate predictions of ice sheet evolution and the interpretation of geological and geodetic observations.

**Acknowledgments.** We thank two anonymous reviewers for their constructive comments, Jerry Mitrovica for insightful discussions, and Douglas Wiens for providing us with the seismic data upon which we based our 3D Earth viscosity model. N. Gomez is funded by the National Science and Engineering Research Council, the Canada Research Chairs Program, the Canadian Foundation for Innovation and McGill University. K. Latychev is supported by the National Aeronautics and Space Administration Grant NNX17AE17G, and

D. Pollard is supported by the National Science Foundation under Grants OCE-1202632 (PLIOMAX) and ANT-1341394. This research is a contribution to the SCAR SERCE program.

## REFERENCES

- A., G., J. Wahr, and S. Zhong, 2013: Computations of the viscoelastic response of a 3-D compressible Earth to surface loading: An application to glacial isostatic adjustment in Antarctica and Canada. *Geophys. J. Int.*, **192**, 557–572, <https://doi.org/10.1093/gji/ggs030>.
- Alley, R. B., S. Anandakrishnan, K. Christianson, H. J. Horgan, A. Muto, B. R. Parizek, D. Pollard, and R. T. Walker, 2015: Oceanic forcing of ice-sheet retreat: West Antarctica and more. *Annu. Rev. Earth Planet. Sci.*, **43**, 207–231, <https://doi.org/10.1146/annurev-earth-060614-105344>.
- An, M., and Coauthors, 2015a: Temperature, lithosphere–asthenosphere boundary, and heat flux beneath the Antarctic Plate inferred from seismic velocities. *J. Geophys. Res. Solid Earth*, **120**, 8720–8742, <https://doi.org/10.1002/2015JB011917>.
- , and Coauthors, 2015b: S-velocity model and inferred Moho topography beneath the Antarctic Plate from Rayleigh waves. *J. Geophys. Res. Solid Earth*, **120**, 359–383, <https://doi.org/10.1002/2014JB011332>.
- Austermann, J., J. X. Mitrovica, K. Latychev, and G. A. Milne, 2013: Barbados-based estimate of ice volume at Last Glacial Maximum affected by subducted plate. *Nat. Geosci.*, **6**, 553–557, <https://doi.org/10.1038/ngeo1859>.
- Bradley, S. L., R. C. A. Hindmarsh, P. L. Whitehouse, M. J. Bentley, and M. A. King, 2015: Low post-glacial rebound rates in the Weddell Sea due to late Holocene ice-sheet readvance. *Earth Planet. Sci. Lett.*, **413**, 79–89, <https://doi.org/10.1016/j.epsl.2014.12.039>.
- Briggs, R. D., D. Pollard, and L. Tarasov, 2013: A glacial systems model configured for large ensemble analysis of Antarctic deglaciation. *Cryosphere*, **7**, 1949–1970, <https://doi.org/10.5194/tc-7-1949-2013>.
- Cande, S. C., J. M. Stock, R. D. Müller, and T. Ishihara, 2000: Cenozoic motion between East and West Antarctica. *Nature*, **404**, 145–150, <https://doi.org/10.1038/35004501>.
- Chaput, J., and Coauthors, 2014: The crustal thickness of West Antarctica. *J. Geophys. Res. Solid Earth*, **119**, 378–395, <https://doi.org/10.1002/2013JB010642>.
- Conrad, C. P., and C. Lithgow-Bertelloni, 2006: Influence of continental roots and asthenosphere on plate-mantle coupling. *Geophys. Res. Lett.*, **33**, L05312, <https://doi.org/10.1029/2005GL025621>.
- Dalziel, I. W. D., and L. A. Lawver, 2001: The lithospheric setting of the West Antarctic Ice Sheet. *The West Antarctic Ice Sheet: Behavior and Environment*, R. B. Alley and R. A. Bindshadler, Antarctic Research Series, Vol. 77, Amer. Geophys. Union, 29–44, <https://doi.org/10.1029/AR077p0029>.
- Danesi, S., and A. Morelli, 2001: Structure of the upper mantle under the Antarctic Plate from surface wave tomography. *Geophys. Res. Lett.*, **28**, 4395–4398, <https://doi.org/10.1029/2001GL013431>.
- de Boer, B., P. Stocchi, and R. S. W. van de Wal, 2014: A fully coupled 3-D ice-sheet–sea-level model: Algorithm and applications. *Geosci. Model Dev.*, **7**, 2141–2156, <https://doi.org/10.5194/gmd-7-2141-2014>.



- DeConto, R. M., and D. Pollard, 2016: Contribution of Antarctica to past and future sea-level rise. *Nature*, **531**, 591–597, <https://doi.org/10.1038/nature17145>.
- Dziewonski, A. M., and D. L. Anderson, 1981: Preliminary reference Earth model. *Phys. Earth Planet. Inter.*, **25**, 297–356, [https://doi.org/10.1016/0031-9201\(81\)90046-7](https://doi.org/10.1016/0031-9201(81)90046-7).
- Fastook, J. L., and M. Prentice, 1994: A finite-element model of Antarctica: Sensitivity test for meteorological mass–balance relationship. *J. Glaciol.*, **40**, 167–175, <https://doi.org/10.1017/S0022143000003944>.
- Fretwell, P., and Coauthors, 2013: Bedmap2: Improved ice bed, surface and thickness datasets for Antarctica. *Cryosphere*, **7**, 375–393, <https://doi.org/10.5194/tc-7-375-2013>.
- Goldberg, S. L., H. C. P. Lau, J. X. Mitrovica, and K. Letychev, 2016: The timing of the Black Sea flood event: Insights from modeling of glacial isostatic adjustment. *Earth Planet. Sci. Lett.*, **452**, 178–184, <https://doi.org/10.1016/j.epsl.2016.06.016>.
- Golledge, N. R., D. E. Kowalewski, T. R. Naish, R. H. Levy, C. J. Fogwill, and E. G. W. Gasson, 2015: The multi-millennial Antarctic commitment to future sea-level rise. *Nature*, **526**, 421–425, <https://doi.org/10.1038/nature15706>.
- Gomez, N., J. X. Mitrovica, P. Huybers, and P. U. Clark, 2010: Sea level as a stabilizing factor for marine-ice-sheet grounding lines. *Nat. Geosci.*, **3**, 850–853, <https://doi.org/10.1038/ngeo1012>.
- , D. Pollard, J. X. Mitrovica, P. Huybers, and P. U. Clark, 2012: Evolution of a coupled marine ice sheet–sea level model. *J. Geophys. Res.*, **117**, F01013, <https://doi.org/10.1029/2011JF002128>.
- , —, and —, 2013: A 3-D coupled ice sheet–sea level model applied to Antarctica over the last 40 ky. *Earth Planet. Sci. Lett.*, **384**, 88–99, <https://doi.org/10.1016/j.epsl.2013.09.042>.
- , —, and D. Holland, 2015: Sea-level feedback lowers projections of future Antarctic Ice-Sheet mass loss. *Nat. Commun.*, **6**, 8798, <https://doi.org/10.1038/ncomms9798>.
- Hansen, S. E., and Coauthors, 2014: Imaging the Antarctic mantle using adaptively parameterized P-wave tomography: Evidence for heterogeneous structure beneath West Antarctica. *Earth Planet. Sci. Lett.*, **408**, 66–78, <https://doi.org/10.1016/j.epsl.2014.09.043>.
- Harley, S. L., 2003: Archaeoan-Cambrian crustal development of East Antarctica: Metamorphic characteristics and tectonic implications. *Geol. Soc. of London Special Publ.*, **206**, 203–230, <https://doi.org/10.1144/GSL.SP.2003.206.01.11>.
- Hay, C., J. X. Mitrovica, N. Gomez, J. R. Creveling, J. Austermann, and R. E. Kopp, 2014: The sea-level fingerprints of ice-sheet collapse during interglacial periods. *Quat. Sci. Rev.*, **87**, 60–69, <https://doi.org/10.1016/j.quascirev.2013.12.022>.
- , H. C. P. Lau, N. Gomez, J. Austermann, E. Powell, J. X. Mitrovica, K. Letychev, and D. A. Wiens, 2017: Sea level fingerprints in a region of complex Earth structure: The case of WAIS. *J. Climate*, **30**, 1881–1892, <https://doi.org/10.1175/JCLI-D-16-0388.1>.
- Heeszel, D. S., D. A. Wiens, A. A. Nyblade, S. E. Hansen, M. Kanao, M. An, and Y. Zhao, 2013: Rayleigh wave constraints on the structure and tectonic history of the Gamburtsev Subglacial Mountains, East Antarctica. *J. Geophys. Res. Solid Earth*, **118**, 2138–2153, <https://doi.org/10.1002/jgrb.50171>.
- , and Coauthors, 2016: Upper mantle structure of the central and West Antarctica from array analysis of Rayleigh wave phase velocities. *J. Geophys. Res. Solid Earth*, **121**, 1758–1775, <https://doi.org/10.1002/2015JB012616>.
- Hjort, C., Ó. Ingólfsson, P. Möller, and J. M. Lirio, 1997: Holocene glacial history and sea-level changes on James Ross Island, Antarctic Peninsula. *J. Quat. Sci.*, **12**, 259–273, [https://doi.org/10.1002/\(SICI\)1099-1417\(199707/08\)12:4<259::AID-JQS307>3.0.CO;2-6](https://doi.org/10.1002/(SICI)1099-1417(199707/08)12:4<259::AID-JQS307>3.0.CO;2-6).
- IAG/SCAR-SERCE, 2017: Report on IAG/SCAR-SERCE Workshop on Glacial Isostatic Adjustment and Elastic Deformation Reykjavik, 5–7th September 2017. Scientific Committee on Antarctic Research Rep., <https://www.scar.org/scar-news/serce-news/report-on-iag-workshop/>.
- Ivins, E. R., T. S. James, J. Wahr, E. J. O. Schrama, F. W. Landerer, and K. M. Simon, 2013: Antarctic contribution to sea level rise observed by GRACE with improved GIA correction. *J. Geophys. Res. Solid Earth*, **118**, 3126–3141, <https://doi.org/10.1002/jgrb.50208>.
- Jordan, T. A., F. Ferraccioli, D. G. Vaughan, J. W. Holt, H. Corr, D. D. Blankenship, and T. M. Diehl, 2010: Aerogravity evidence for major crustal thinning under the Pine Island Glacier region (West Antarctica). *Geol. Soc. Amer. Bull.*, **122**, 714–726, <https://doi.org/10.1130/B26417.1>.
- Joughin, I., B. E. Smith, and B. Medley, 2014: Marine ice sheet collapse potentially under way for the Thwaites Glacier Basin, West Antarctica. *Science*, **344**, 735–738, <https://doi.org/10.1126/science.1249055>.
- Kaufmann, G., P. Wu, and E. R. Ivins, 2005: Lateral viscosity variations beneath Antarctica and their implications on regional rebound motions and seismotectonics. *J. Geodyn.*, **39**, 165–181, <https://doi.org/10.1016/j.jog.2004.08.009>.
- Kendall, R. A., J. X. Mitrovica, and G. A. Milne, 2005: On post-glacial sea level—II. Numerical formulation and comparative results on spherically symmetric models. *Geophys. J. Int.*, **161**, 679–706, <https://doi.org/10.1111/j.1365-246X.2005.02553.x>.
- Konrad, H., M. Thoma, I. Sasgen, V. Klemann, K. Grosfeld, D. Barbi, and Z. Martinec, 2014: The deformational response of a viscoelastic solid Earth model coupled to a thermomechanical ice sheet model. *Surv. Geophys.*, **35**, 1441–1458, <https://doi.org/10.1007/s10712-013-9257-8>.
- , I. Sasgen, D. Pollard, and V. Klemann, 2015: Potential of the solid-Earth response for limiting long-term West Antarctic Ice Sheet retreat in a warming climate. *Earth Planet. Sci. Lett.*, **432**, 254–264, <https://doi.org/10.1016/j.epsl.2015.10.008>.
- Kopp, R. E., F. J. Simons, J. X. Mitrovica, A. C. Maloof, and M. Oppenheimer, 2013: A probabilistic assessment of sea level variations within the last interglacial stage. *Geophys. J. Int.*, **193**, 711–716, <https://doi.org/10.1093/gji/ggt029>.
- Lambeck, K., C. Smither, and P. Johnston, 1998: Sea-level change, glacial rebound and mantle viscosity for northern Europe. *Geophys. J. Int.*, **134**, 102–144, <https://doi.org/10.1046/j.1365-246x.1998.00541.x>.
- , H. Rouby, A. Purcell, Y. Sun, and M. Sambridge, 2014: Sea level and global ice volumes from the Last Glacial Maximum to the Holocene. *Proc. Natl. Acad. Sci. USA*, **111**, 15 296–15 303, <https://doi.org/10.1073/pnas.1411762111>.
- Letychev, K., J. X. Mitrovica, J. Tromp, M. E. Tamisiea, D. Komatitsch, and C. C. Christara, 2005: Glacial isostatic adjustment on 3-D Earth models: A finite-volume formulation. *Geophys. J. Int.*, **161**, 421–444, <https://doi.org/10.1111/j.1365-246X.2005.02536.x>.
- Le Meur, E., and P. Huybrechts, 2001: A model computation of the temporal changes of surface gravity and geoidal signal induced by the evolving Greenland ice sheet. *Geophys. J. Int.*, **145**, 835–849, <https://doi.org/10.1046/j.1365-246x.2001.01442.x>.
- Mercer, J. H., 1968: Antarctic ice and Sangamon sea level. *Int. Assoc. Sci. Hydrol. Publ.*, **79**, 217–225.
- , 1978: West Antarctic Ice Sheet and CO<sub>2</sub> greenhouse effect: A threat of disaster. *Nature*, **271**, 321–325, <https://doi.org/10.1038/271321a0>.

- Mitrovica, J. X., and A. M. Forte, 2004: A new inference of mantle viscosity based upon joint inversion of convection and glacial isostatic adjustment data. *Earth Planet. Sci. Lett.*, **225**, 177–189, <https://doi.org/10.1016/j.epsl.2004.06.005>.
- Morelli, A., and S. Danesi, 2004: Seismological imaging of the Antarctic continental lithosphere: A review. *Global Planet. Change*, **42**, 155–165, <https://doi.org/10.1016/j.gloplacha.2003.12.005>.
- Peltier, W. R., 1974: The impulse response of a Maxwell Earth. *Rev. Geophys.*, **12**, 649–669, <https://doi.org/10.1029/RG012i004p00649>.
- , 2004: Global glacial isostasy and the surface of the ice-age Earth: The ICE-5G (VM2) model and GRACE. *Annu. Rev. Earth Planet. Sci.*, **32**, 111–149, <https://doi.org/10.1146/annurev.earth.32.082503.144359>.
- , D. F. Argus, and R. Drummond, 2015: Space geodesy constrains Ice Age terminal deglaciation: The global ICE-6G\_C (VM5a) model. *J. Geophys. Res. Solid Earth*, **120**, 450–487, <https://doi.org/10.1002/2014JB011176>.
- Pollard, D., and R. M. DeConto, 2009: Modelling West Antarctic Ice Sheet growth and collapse through the past five million years. *Nature*, **458**, 329–332, <https://doi.org/10.1038/nature07809>.
- , and —, 2012: Description of a hybrid ice sheet–shelf model, and application to Antarctica. *Geosci. Model Dev.*, **5**, 1273–1295, <https://doi.org/10.5194/gmd-5-1273-2012>.
- , —, and R. B. Alley, 2015: Potential Antarctic Ice Sheet retreat driven by hydrofracturing and ice cliff failure. *Earth Planet. Sci. Lett.*, **412**, 112–121, <https://doi.org/10.1016/j.epsl.2014.12.035>.
- , W. Chang, M. Haran, P. Applegate, and R. DeConto, 2016: Large ensemble modeling of last deglacial retreat of the West Antarctic Ice Sheet: Comparison of simple and advanced statistical techniques. *Geosci. Model Dev.*, **9**, 1697–1723, <https://doi.org/10.5194/gmd-9-1697-2016>.
- , N. Gomez, and R. DeConto, 2017: Variations of the Antarctic Ice Sheet in a coupled ice sheet–Earth–sea level model: Sensitivity to viscoelastic Earth properties. *J. Geophys. Res. Earth Surf.*, **122**, 2124–2138, <https://doi.org/10.1002/2017JF004371>.
- Ramirez, C., and Coauthors, 2016: Crustal and upper-mantle structure beneath ice-covered regions in Antarctica from *S*-wave receiver functions and implications for heat flow. *Geophys. J. Int.*, **204**, 1636–1648, <https://doi.org/10.1093/gji/ggv542>.
- Rignot, E., J. Mouginot, M. Morlighem, H. Seroussi, and B. Scheuchl, 2014: Widespread, rapid grounding line retreat of Pine Island, Thwaites, Smith, and Kohler glaciers, West Antarctica, from 1992 to 2011. *Geophys. Res. Lett.*, **41**, 3502–3509, <https://doi.org/10.1002/2014GL060140>.
- Ritsema, J., A. Deuss, H. van Heijst, and J. Woodhouse, 2011: S40RTS: A degree-40 shear-velocity model for the mantle from new Rayleigh wave dispersion, teleseismic traveltime and normal-mode splitting function measurements. *Geophys. J. Int.*, **184**, 1223–1236, <https://doi.org/10.1111/j.1365-246X.2010.04884.x>.
- Ritzwoller, M. H., N. M. Shapiro, A. L. Levshin, and G. M. Leahy, 2001: Crustal and upper mantle structure beneath Antarctica and surrounding oceans. *J. Geophys. Res.*, **106**, 30 645–30 670, <https://doi.org/10.1029/2001JB000179>.
- Roberts, S. J., and Coauthors, 2011: Geological constraints on glacio-isostatic adjustment models of relative sea-level change during deglaciation of Prince Gustav Channel, Antarctic Peninsula. *Quat. Sci. Rev.*, **30**, 3603–3617, <https://doi.org/10.1016/j.quascirev.2011.09.009>.
- Shapiro, N. M., and M. H. Ritzwoller, 2004: Inferring surface heat flux distributions guided by a global seismic model: Particular application to Antarctica. *Earth Planet. Sci. Lett.*, **223**, 213–224, <https://doi.org/10.1016/j.epsl.2004.04.011>.
- Siebert, M., N. Ross, H. Corr, J. Kingslake, and R. Hindmarsh, 2013: Late Holocene ice-flow reconfiguration in the Weddell Sea sector of West Antarctica. *Quat. Sci. Rev.*, **78**, 98–107, <https://doi.org/10.1016/j.quascirev.2013.08.003>.
- Thompson, W. G., H. A. Curran, M. A. Wilson, and B. White, 2011: Sea-level oscillations during the last interglacial highstand recorded by Bahamas corals. *Nat. Geosci.*, **4**, 684–687, <https://doi.org/10.1038/ngeo1253>.
- van der Wal, W., P. L. Whitehouse, and E. J. O. Schrama, 2015: Effect of GIA models with 3D composite mantle viscosity on GRACE mass balance estimates for Antarctica. *Earth Planet. Sci. Lett.*, **414**, 134–143, <https://doi.org/10.1016/j.epsl.2015.01.001>.
- Weertman, J., 1974: Stability of the junction of an ice sheet and an ice shelf. *J. Glaciol.*, **13**, 3–11, <https://doi.org/10.1017/S0022143000023327>.
- Whitehouse, P. L., M. J. Bentley, G. A. Milne, M. A. King, and I. D. Thomas, 2012: A new glacial isostatic model for Antarctica: Calibrated and tested using observations of relative sea-level change and present-day uplifts. *Geophys. J. Int.*, **190**, 1464–1482, <https://doi.org/10.1111/j.1365-246X.2012.05557.x>.
- Wu, P., and W. van der Wal, 2003: Postglacial sealevels on a spherical, self-gravitating viscoelastic earth: Effects of lateral viscosity variations in the upper mantle on the inference of viscosity contrasts in the lower mantle. *Earth Planet. Sci. Lett.*, **211**, 57–68, [https://doi.org/10.1016/S0012-821X\(03\)00199-7](https://doi.org/10.1016/S0012-821X(03)00199-7).